



# Structural, optical and photoluminescence properties of $K_{0.5}Na_{0.5}NbO_3$ ceramics synthesized by sol–gel reaction method

Shammi Kumar<sup>1</sup> · Mamta Shandilya<sup>2</sup> · Shweta Thakur<sup>3</sup> · Nagesh Thakur<sup>1</sup>

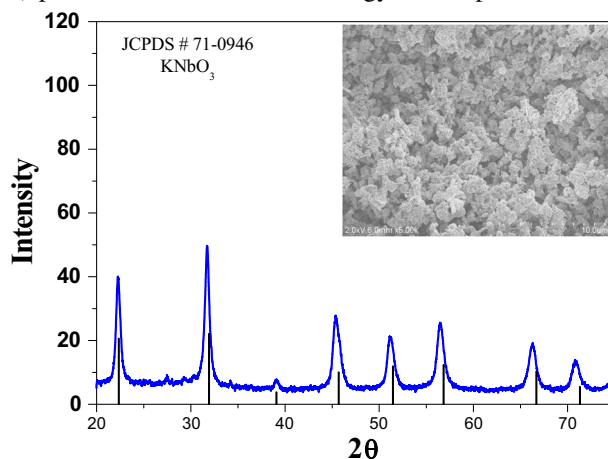
Received: 21 June 2018 / Accepted: 23 August 2018 / Published online: 3 September 2018  
© Springer Science+Business Media, LLC, part of Springer Nature 2018

## Abstract

Potassium sodium niobate (KNN) ceramics have been prepared by sol–gel route. The effect of conventional sintering on its optical and photoluminescence properties has been studied. Optical measurements were done by reflectance measurements of the ceramics which showed decrease in optical band gap energy with an increase in sintering temperature. A room temperature photoluminescence (PL) spectrum was taken at an excitation wavelength of 300 nm. The existence of green emission confirms the existence of oxygen vacancies in the sample. Raman spectroscopy analysis revealed changes in Raman scattering mode for KNN ceramics sintered at different temperatures.  $I$ – $V$  characteristics have been studied from 20–180 V disclosed that increase in sintering temperature favor higher order of leakage current at room temperature.

## Graphical Abstract

The intense peaks around  $2\theta = 22.27^\circ, 31.78^\circ, 39.14^\circ, 45.49^\circ, 51.26^\circ, 56.60^\circ, 66.42^\circ, 70.96^\circ,$  and  $75.39^\circ$  prove the perovskite structure of KNN powder. The peaks observed around  $22^\circ, 31^\circ,$  and  $46^\circ$  revealed that KNN has a pure perovskite orthorhombic structure with single phase which is indexed according to JCPDS card number 71–0946 ( $KNbO_3$ ). The (110) plane has high intensity than (100) plane due its low surface energy as compared to other lattice planes.



✉ Mamta Shandilya  
mamta2882@gmail.com

<sup>1</sup> Department of Physics, Himachal Pradesh University, Shimla, HP, India

<sup>2</sup> School of Physics and Materials Science, Shoolini University, Solan, HP 173229, India

<sup>3</sup> I3N-Aveiro, Department of Physics, University of Aveiro, Aveiro 3810 193, Portugal

## Highlights

- A polycrystalline KNN precursor solution has been prepared by using sodium acetate, potassium acetate and niobium pentaethoxide as initial chemical reagents using sol–gel method.
- The pure phase XRD pattern of KNN powder calcined at 750 °C was achieved and SEM clear that fine and homogeneous powder was formed.
- Raman spectroscopy analysis was done to study the extent of crystallization and Raman scattering mode during temperature variation in the sample which is good in this sample.
- The values of optical band gap energies are 3.27 eV and 3.17 eV for KNN-850 and KNN-1050, respectively. This revealed that optical band gap energy decreases with increase in sintering temperature due to increase in crystallite size and formation of intermediate energy levels.
- PL spectra have an emission band in UV/visible region, which explore their application fields of electro-optics devices. *I–V* characteristics showed that KNN samples have linear ohmic and SCLC conduction mechanisms at higher applied electric voltages.

**Keywords** KNN · XRD · Raman spectra · Photoluminescence spectrum · *I–V* characteristics

## 1 Introduction

Smart structure materials have improved the efficiency in the performance of optoelectronic devices like solar cells, light-emitting diodes (LEDs), photo-detectors and lasers. An organic and inorganic hybrid perovskites (OIHPs) have emerged as an important group of functional materials for applications in high-performance [1, 2]. The impressive wide-ranging performance of OIHP devices in these applications is ascribed to a significant set of optoelectronic properties, together with tunable optical bandgaps, high optical extinction coefficients, high charge carrier mobility and long carrier diffusion length. In addition, photoluminescence properties of these phosphors are dependent on not only crystal structure, but also upon preparation condition of the samples [3, 4]. But the use of PbO in halide materials are though compatible with human bodies and the environment, but their disposable and recycling become difficult because of the formation of Lead oxide (PbO) during thermal treatments [5]. In order to replace Pb-based materials and find an alternate, many attempts have been made in the past to find out new materials whose properties are compatible or more advanced than Pb-based materials. Scientists have till date reported numerous Pb-free piezoelectric materials, but KNN among all is only considered as a very potential candidate to replace PZT materials. Polycrystalline KNN material is a solid solution of antiferroelectric sodium niobate (NN) and ferroelectric potassium niobate (KN) which has high Curie temperature, environment-friendly composition and excellent piezoelectric properties [6, 7]. The trouble in the preparation of KNN ceramics is the volatile nature of sodium and potassium metal ions during calcinations and sintering processes. In KNN ceramics, the volatile nature of alkaline ions give rise to defects states such as alkaline vacancies, oxygen vacancies, and space charge carriers. These defects in

polycrystalline materials interact with domain walls and give rise to poor electrical properties [8]. Due to these defects states, it becomes a tedious task to obtain the desired stoichiometry and high density defect free materials. In order to control and overcome these losses many dopants and excessive amounts of alkali metal ions (Na, K) are added [9]. Additionally the use of sol–gel method instead of conventional solid-state reaction (SSR) method is fit for the synthesis of KNN because of the high interdiffusion of cations, low production temperature, control of stoichiometry at molecular level, and low particle size.

In this paper, we study the effect of conventional sintering technique on phase structure, electrical and optical properties of  $K_{0.5}Na_{0.5}NbO_3$  ceramics. A detailed and comparative study has been made on KNN ceramics sintered at different temperatures. To the best of our knowledge, a very few reports have been made on the defect states, band gap, optical and luminescence properties of  $K_{0.5}Na_{0.5}NbO_3$  ceramics.

## 2 Materials and methods

A polycrystalline KNN precursor solution has been prepared by using sodium acetate (Sigma-Aldrich, 99.99%), potassium acetate (Sigma-Aldrich, 99.00%) and niobium pentaethoxide (Sigma-Aldrich, 99.95%) as initial chemical reagents. These initial chemical reagents were weighed according to composition  $K_{0.5}Na_{0.5}NbO_3$  and dissolved in solvent, 2-methoxyethanol to form a clear precursor solution. Acetyl acetone was added to the solution which is acting as a chelating agent. 20% excessive amounts of alkali acetate (Na, K) were added to overcome their losses during calcinations and sintering processes. The prepared solution was stirred at 90 °C for 4 h to prepare clear and homogeneous solution. After that synthesized KNN solution was

dried at 100 °C for 1 h to form a dark-brown-colored powder. Finally, KNN solution was calcined at 750 °C for 1 h to form pure white crystalline phase. To form highly dense material, KNN pellets were prepared by applying a pressure of 3 tons. These pellets were sintered at 850 and 1050 °C for 2 h in a conventional furnace by using silica crucible. The phase determination of KNN ceramic was analyzed by X-ray diffractometer (Philips X'pert Pro) by using Cu-K $\alpha$  radiations of wavelength 1.54 Å. Phonon vibration properties were studied by using Raman spectrometer RIRM model (RI Instruments & Innovation India). Optical and PL measurements were done by using a Perkin-Elmer lambda 750 spectrophotometer and Perkin Elmer LS55 fluorescence spectrometer, respectively.

### 3 Results and discussion

#### 3.1 Crystallinity study

Figure 1 shows the XRD pattern of KNN powder calcined at 750 °C by using a step scanning method with the following conditions; 2 $\theta$ : 20°–80°, step width: 0.02° and counting rate of 6 s. The intense peaks around 2 $\theta$  = 22.27°, 31.78°, 39.14°, 45.49°, 51.26°, 56.60°, 66.42°, 70.96°, and 75.39° correspond to the reflection of crystal planes of KNN powder. No other diffraction peaks are found in the XRD

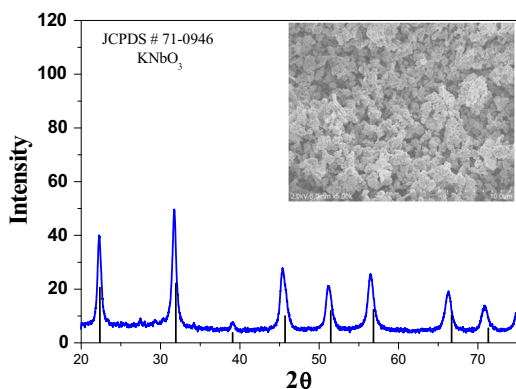


Fig. 1 XRD pattern of KNN powder calcined at 750 °C

**Table 1** Lattice parameters of KNN ceramic calcined at 700 °C

Sample	Crystal system	Lattice parameter (Å)	Volume (Å) <sup>3</sup>	$d_{\text{obs}}$	$d_{\text{cal}}$	hkl
K <sub>0.5</sub> Na <sub>0.5</sub> NbO <sub>3</sub>	Orthorhombic	$a = 3.98693$	63.205 $c/a$ Ratio = 1.006	3.4963	3.4635	110
		$b = 3.97182$		2.2465	2.2504	111
		$c = 4.01432$		2.2355	2.2454	021
				1.8862	1.9118	220
				1.7633	1.7710	221
				1.5229	1.6109	202
				1.4476	1.4512	222
				1.2901	1.3291	003
		1.2571	1.2691	420		

pattern which indicate pure phase of KNN sample. The peaks observed around 22°, 31°, and 46° revealed that KNN has a pure perovskite orthorhombic structure with single phase which is indexed according to JCPDS card number 71-0946 (KNbO<sub>3</sub>). The (110) plane has high intensity than (100) plane due its low surface energy as compared to other lattice planes. The non-existence of impurity phases in the XRD pattern confirmed that 20% excessive quantities of alkali metal ions were valuable in controlling the volatilization of Na<sub>2</sub>O and K<sub>2</sub>O at higher calcinations temperature (750 °C). In the inset of Fig. 1 SEM image shows that powder formed by sol-gel technique is very fine and homogeneous. Both XRD and SEM studies support each other. The phase stability and degree of distortion in perovskite ABO<sub>3</sub> structure is estimated in terms of tolerance factor ( $t$ ) which is calculated by using the relation,  $t = \frac{R_A + R_O}{\sqrt{2(R_B + R_O)}}$ , where  $R_A$ ,  $R_B$ , and  $R_O$  are ionic radii of A, B site atoms and of oxygen atom, respectively. The value of  $t$  gives us an idea of up to how much distance, atoms in crystal lattice will move from their ideal packing positions [10, 11]. Generally, the perovskite structures are stable in the range  $0.7 < t < 1.09$ , but, in case of an orthorhombic crystal structure  $t \sim 1$ . In the present case, value of  $t$  is 1.1035 for KNN powder calcined at 750 °C. X-ray density of the sample is calculated by using the relation

$$d_x = \frac{(\text{Sum of atomic weights of all atoms}) \times n}{V \times N} \quad (1)$$

where  $d_x$ ,  $n$ ,  $V$ , and  $N$  are the X-ray density, number of atoms per unit cell, volume of unit cell, and Avogadro's number, respectively. The X-ray density of the sample was 4.503 g/mol calculated by using Eq. (1). The average crystallite size of calcined KNN powder is calculated by using Debye-Scherrer's relation for high intensity reflection line (110) among all peaks in the XRD pattern

$$d = \frac{k\lambda}{\beta \cos \theta} \quad (2)$$

where  $d$  is grain size,  $k$  is Scherrer's constant,  $\lambda$  is wavelength,  $\theta$  is diffracted angle, and  $\beta$  is full width half maxima of diffracted peaks. The values of sub-lattice parameters are shown in Table 1. The crystallite size of the

sample can also be calculated by using Williamson Hall (W–H) plot through the following relation [12, 13]:

$$\beta \cos \theta = \frac{K\lambda}{D} + 4 \sin \theta \quad (3)$$

where  $D$  is the grain size and  $\sigma$  is the lattice strain. A plot between  $4\sigma \sin \theta$  and  $\beta \cos \theta$  is shown in Fig. 2. Crystallite size and lattice strain were calculated from the linear fitting of the curve. The observed value of lattice strain ( $\sigma$ ) is  $2.91 \times 10^{-3}$ . The value of crystallite size and dislocation density are shown in Table 2. The value of dislocation density was calculated by using the Williamson and Smallman's relation  $\delta = \frac{n}{D^2}$ , where  $D$  is the grain size and  $n$  is equal to 1 shows minimum dislocation density of the sample [14].

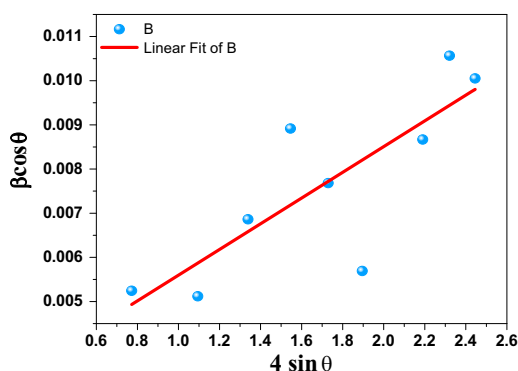


Fig. 2 W–H plot for KNN powder calcined at 750 °C

**Table 2** Crystallite size and dislocation density of KNN power calcined at 750 °C

Sample	Crystallite size (nm)		Dislocation density $\times 10^{14}$	
	Debye–Scherrer's method	W–H plot	Debye–Scherrer's method	W–H plot
$K_{0.5}Na_{0.5}NbO_3$	28	51	3.76	13.71

### 3.2 Internal structure analysis

Raman spectroscopy analysis was done to study the extent of crystallization and Raman scattering mode during temperature variation in the sample. Figure 3 shows the Raman spectrum of KNN ceramics sintered at 850 and 1050 °C in the wave number range 166–1000  $\text{cm}^{-1}$  at room temperature. In KNN-850 °C, the peaks observed around 233, 597, and 846  $\text{cm}^{-1}$  are attributed to triply degenerate symmetric O–Nb–O bending vibration  $\nu_5$  ( $F_{2g}$ ), doubly degenerate symmetric O–Nb–O stretching vibration  $\nu_1$  ( $A_g$ ) and combination of  $\nu_1 + \nu_5$ , respectively due to internal vibration modes of  $NbO_6$  octahedron [15, 16]. With the increase in sintering temperature, intensity of  $\nu_1$  and  $\nu_1 + \nu_5$  vibration modes noticeably increases, which shows better crystallization and perovskite phase in KNN-1050 °C as compared to KNN-850 °C. It is observed that with a rise in temperature, frequencies of  $\nu_1$ ,  $\nu_5$ , and  $\nu_1 + \nu_5$  are shifted towards higher frequency range. In the case of KNN-850 °C,  $\nu_1$ ,  $\nu_5$ , and  $\nu_1 + \nu_5$  vibration modes are observed around 233, 597, and 846  $\text{cm}^{-1}$ . But in the case of KNN-1050 °C,  $\nu_1$ ,  $\nu_5$  and  $\nu_1 + \nu_5$  have scattering position shifted by 10  $\text{cm}^{-1}$  (233–243  $\text{cm}^{-1}$ ), 6  $\text{cm}^{-1}$  (597–603  $\text{cm}^{-1}$ ) and 8  $\text{cm}^{-1}$  (846–854  $\text{cm}^{-1}$ ), respectively. This shift in Raman scattering mode with rise in temperature is related to the compositional variations during higher sintering temperatures.

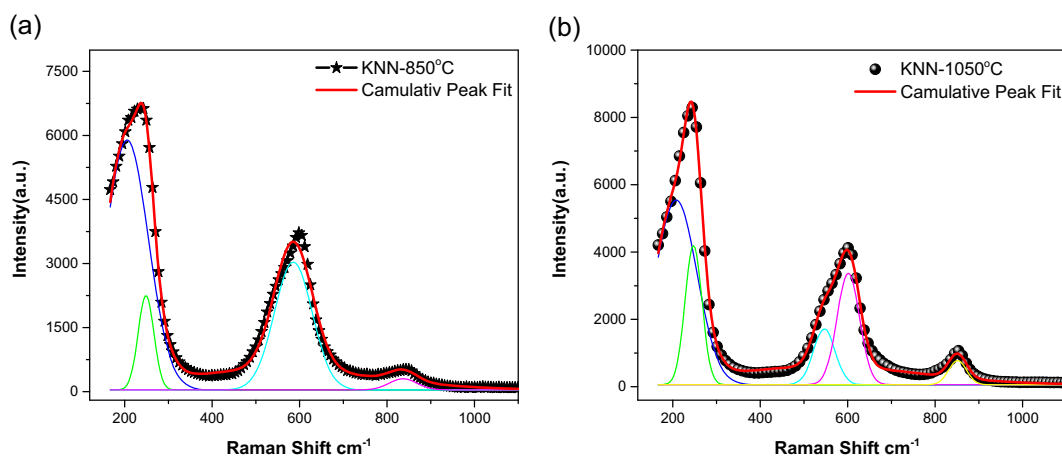


Fig. 3 Raman spectra of KNN powders sintered at 850 and 1050 °C

### 3.3 Optoelectronic properties

Figure 4 shows the reflectance ( $R$ ) spectrum of KNN-850 °C and KNN-1050 °C pellets in the wavelength range of 320–1000 nm. Kubelka–Munk theory is used for investigating the optical band gap energy of samples [17, 18]. According to this theory, Kubelka–Munk function  $F(R)$  is given as

$$F(R) = \frac{1 - R^2}{2R} \tag{4}$$

where  $R$  is reflectance of the material. The value of absorption coefficient ( $\alpha$ ) is calculated by using Eq. (4) as

$$\alpha = \frac{F(R)}{t} \tag{5}$$

where  $t$  denotes thickness of the pellet. The value of the optical band gap energy is calculated by exciting the valence band electrons to the conduction band. The relation

used for finding out optical band energy is as

$$ah\nu = (h\nu - E_g)^n \tag{6}$$

where  $E_g$  is optical band gap,  $\nu$  is the incident photon frequency and the value of  $n$  characterizes which absorption process is involved in the sample, i.e.,  $n = 2$  for indirect band gap transitions and  $n = 1/2$  for direct band gap transitions.

Figure 5 shows graph between  $(\alpha h\nu)^{1/2}$  vs  $h\nu$  to determine the optical band energy of the sample called as Taucplot. The extrapolation of the linear part of  $(\alpha h\nu)^{1/2}$  vs  $h\nu$  curves towards the  $x$ -axis provides optical band gap energy. The values of optical band gap energies are 3.27 eV and 3.17 eV for KNN-850 °C and KNN-1050 °C, respectively. This revealed that optical band gap energy decreases with increase in sintering temperature due to increase in crystallite size and formation of intermediate energy levels. With the rise in sintering temperature, vacancies of alkali

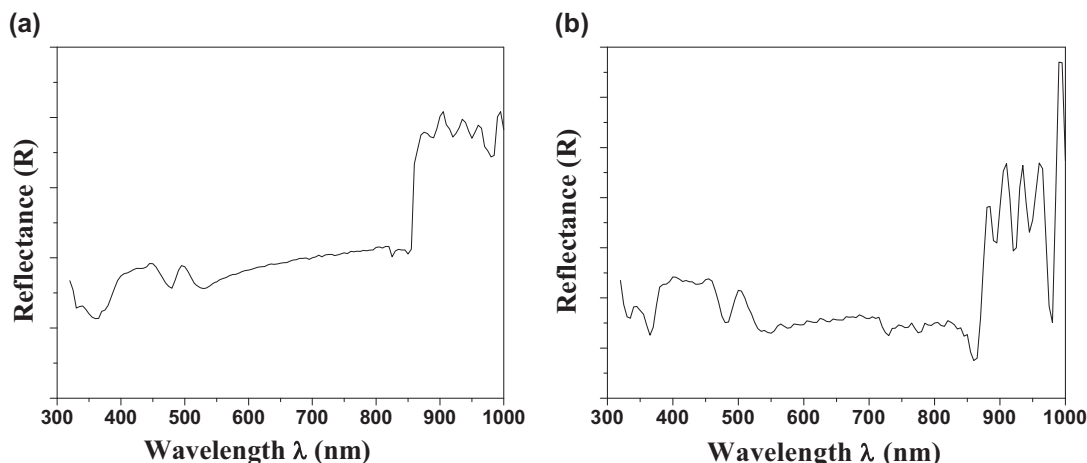


Fig. 4 Reflectance spectra of KNN ceramics sintered at a 850 and b 1050 °C

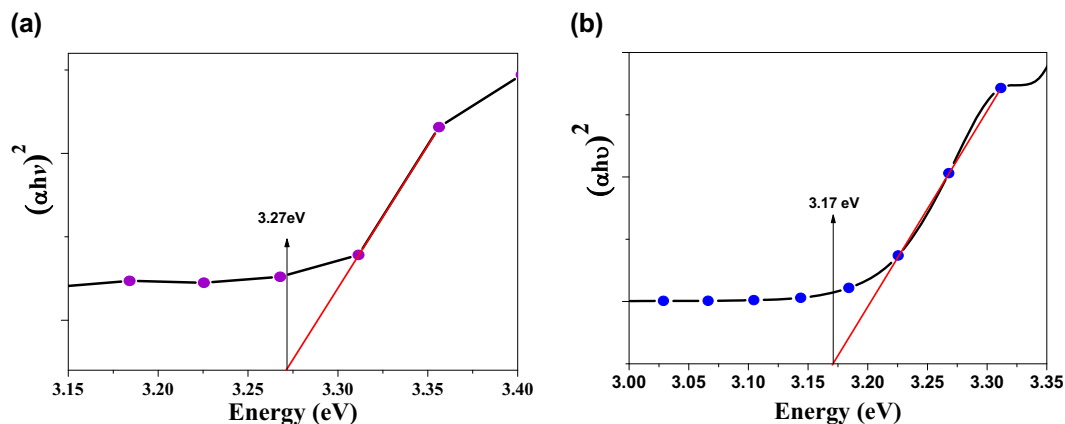


Fig. 5 Plot of  $(\alpha h\nu)^{1/2}$  Vs photon energy at a 850 °C and b 1050 °C

metalions were formed which give rise to the formation of crystal defects and oxygen vacancies. These oxygen vacancies and defect states are responsible for intermediate energy levels and decreased value of optical band gap energy at a higher sintering temperature [19].

Photoluminescence (PL) study is a non-thermal origin process based on spontaneous emission of light during the optical excitation of the sample at room temperature. Figure 6 shows PL spectra of KNN-850 °C and KNN-1050 °C in the wavelength range 300–550 nm at room temperature. The excited wavelength of 300 nm was used to study PL spectra of powder samples. It is observed that samples revealed a broad PL emission spectrum in UV/visible region. Both KNN-850 °C and KNN-1050 °C have three emission bands at room temperature. PL spectrum has peaks around 2.89 and 3.25 eV are related to near band emission (NBE) in the UV region which signifies the band to band transition. The peaks around 2.3–2.5 eV are related to blue/green emission band in the visible region which are

associated with defects in the sample. The emission in green region is usually attributed to oxygen vacancies which increase with rise in sintering temperature. The peak intensity of NBE-declined and of defect peaks increases with sintering temperature, meaning thereby that rise in sintering temperature (>850 °C) increases crystal imperfections and enhanced oxygen vacancies. Defect states emissions bands were observed due to formations of intermediate energy levels caused by formation of oxygen vacancies and crystal defects which give rise to blue/green emission bands. The sharp UV and visible emissions were occurring which disclosed that KNN ceramics may be used for UV/visible laser generation. This PL behavior of KNN leads to their applications in LEDs, optical storage technology and in telecommunication devices.

Figure 7 shows  $I$ - $V$  characteristics of KNN-850 °C and KNN-1050 °C at different applied electric voltages ranging 20–180 V at room temperature. In cases of both the samples, on increasing applied voltages, the value of

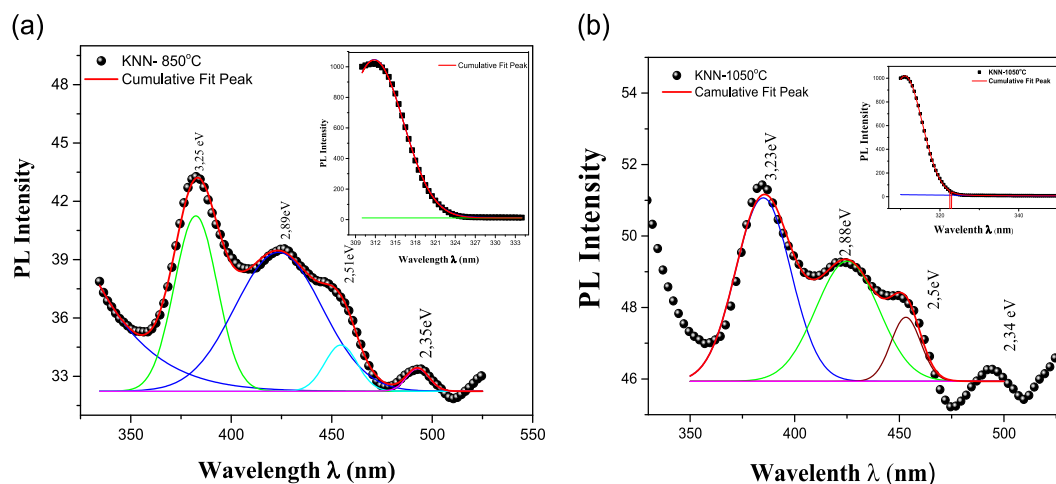


Fig. 6 PL spectrum of KNN ceramics sintered at a 850 °C and b 1050 °C

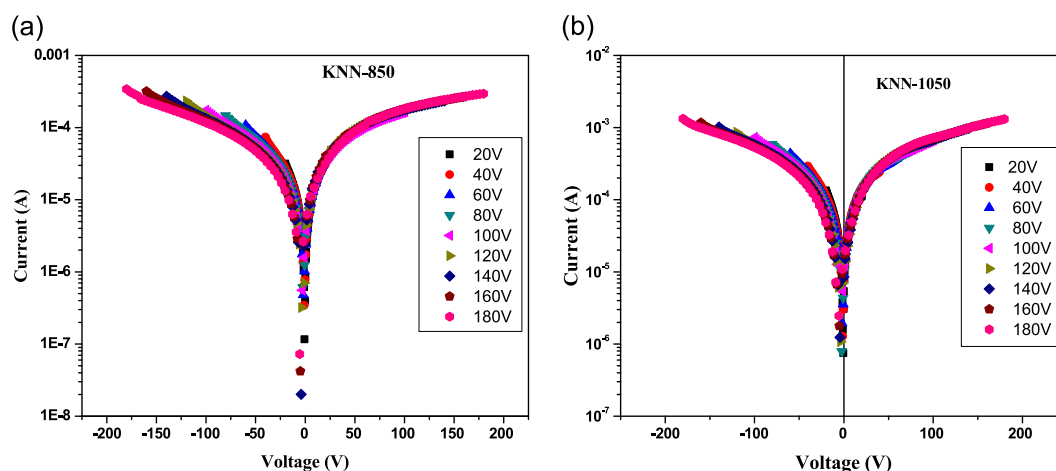


Fig. 7  $I$ - $V$  characteristics of KNN powder sintered at a 850 °C and b 1050 °C



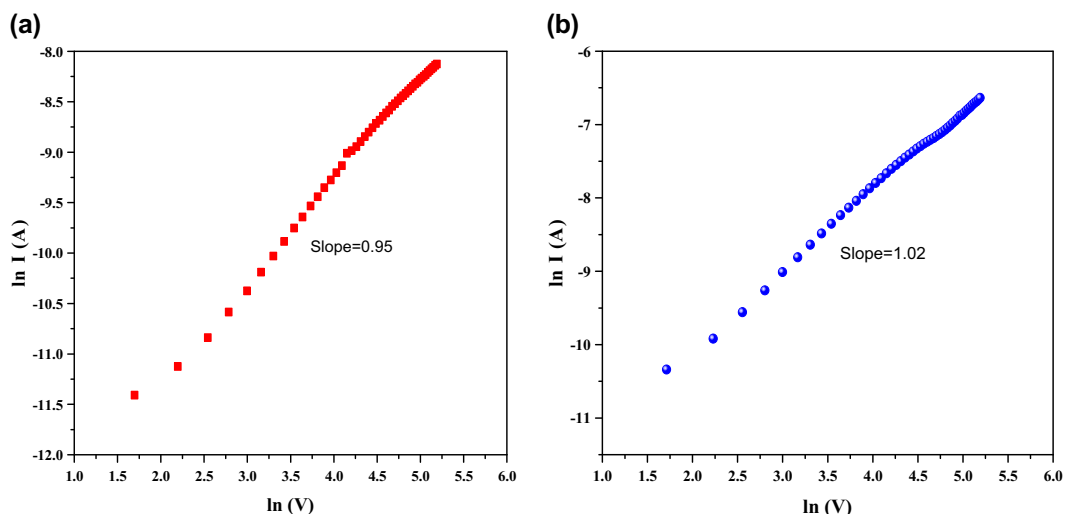


Fig. 8 Graph between  $\ln I$  vs  $\ln V$  for SCLC mechanism a KNN-850 and b KNN-1050

leakage current ( $I$ ) increases drastically due to formations of (K, Na) ions vacancies and defect states at higher sintering temperature. The presence of oxygen vacancies formed by evaporation of (Na, K) ions are liable for the increase in the value of leakage current at higher applied electric voltages [20]. In KNN-850 °C, the order of leakage current varied from  $2.08 \times 10^{-8}$ – $3.49 \times 10^{-4}$  A and in KNN-1050 °C, order of leakage current varied from  $7.38 \times 10^{-7}$ – $1.37 \times 10^{-3}$  A. We have observed that increase in sintering temperature give rise to increase in leakage current due to increase in oxygens vacancies.

Figure 8a, b shows the variation of  $\ln(I)$  with  $\ln(V)$  for KNN-850 °C and KNN-1050 °C, respectively. The linear curve is obtained at higher electric voltages. The value of slope becomes close to 1 with increase in electric voltages which showed that the sample has linear ohmic conduction at higher electric fields. The value of slopes starts increasing and curves become almost linear at higher electric voltages, which may give an indication of the other possible conduction mechanism. Thus, to know the other conduction mechanism at higher electric voltages, the curves between  $\ln(I)$  Vs  $V^{1/2}$  are drawn for both KNN-850 °C and KNN-1050 °C samples. The values of dielectric constant ( $K$ ) for both Poole–Frenkel (P–F) and Schottky–Emission (S–E) mechanisms are calculated by using Eq. (7):

$$I = I_0 \exp\left(\beta V^{1/2}/kT\right) \tag{7}$$

where  $I_0$  is a constant,  $V$  is voltage,  $k$  is Boltzmann’s constant,  $T$  is absolute temperature and  $\beta$  is a constant which is given as

$$\beta = \left(\frac{e^3}{\alpha\pi K \epsilon_0}\right)^{1/2} \tag{8}$$

where  $K$  is dielectric constant,  $e$  is electron charge, and  $\epsilon_0$  is permittivity of free space. The value of  $\alpha = 1$  and 4, for P–F and S–E, respectively. In the case of KNN-850 °C, the calculated values of  $K$  from the slope of linear fitting are 0.0243 and 0.00607 for P–E and S–E mechanisms, respectively. Similarly, for KNN-1050 °C the values of  $K$  are 0.0138 and 0.00345 for P–E and S–E mechanisms, respectively. The value of  $K$  for KNN materials lies between the optical dielectric constant i.e., 5 and static dielectric constant i.e., 1000 [21]. Thus, in the present case, calculated values of  $K$  in both P–E and S–E mechanisms are outside this range which demonstrate that only ohmic and SCLC mechanisms are dominated up to 200 V at room temperature.

### 4 Conclusion

KNN ceramics have been synthesized successively by sol-gel route. XRD analysis revealed perovskite orthorhombic crystal structure at room temperature. Raman spectroscopy analysis revealed that increase in sintering temperature gives rise to change in frequency of internal vibration modes and gives better crystallization. Optical study revealed a decrease in optical band gap energy with increase in sintering temperature. PL spectra have an emission band in UV/visible region, which explore their application fields of electro-optics devices.  $I$ – $V$  characteristics showed that KNN samples have linear ohmic and SCLC conduction mechanisms at higher applied electric voltages.

### Compliance with ethical standards

**Conflict of interest** The authors declare that they have no conflict of interest.

## References

1. Jeon NJ, Noh JH, Yang WS, Kim YC, Ryu S, Seo J et al. (2015) Compositional engineering of perovskite materials for high-performance solar cells. *Nature* 517:476
2. Fang Y, Huang J (2015) Resolving weak light of sub- $\mu\text{m}^2$  per square centimeter by hybrid perovskite photodetectors enabled by noise reduction. *Adv Mater* 27:2804–10
3. Bella F, Griffini G, Correa-Baena J-P, Saracco G, Grätzel M, Hagfeldt A et al. (2016) Improving efficiency and stability of perovskite solar cells with photocurable fluoropolymers. *Science* 354:203–6
4. Zhu H, Fu Y, Meng F, Wu X, Gong Z, Ding Q et al. (2015) Lead halide perovskite nanowire lasers with low lasing thresholds and high quality factors. *Nat Mater* 14:636
5. Ibanez JG, Rincoán ME, Gutierrez-Granados S, Chahma MÁ, Jaramillo-Quintero OA, Frontana-Urbe BA (2018) Conducting polymers in the fields of energy, environmental remediation, and chemical, chiral sensors. *Chem Rev* 118:4731–816
6. Zhang M-H, Wang K, Du Y-J, Dai G, Sun W, Li G et al. (2017) High and temperature-insensitive piezoelectric strain in alkali niobate lead-free perovskite. *J Am Chem Soc* 139:3889–95
7. Lu X, Hou L, Jin L, Wang L, Tian Y, Yu K et al. (2017) Structure evolution and exceptionally ultra-low hysteresis unipolar electric field-induced strain in  $(1-x)\text{NaNbO}_3-x\text{BaTiO}_3$  lead-free ferroelectrics. *Ceram Int* 44:5492–5499
8. Rafiq MA, Costa ME, Tkach A, Vilarinho PM (2015) Impedance analysis and conduction mechanisms of lead free potassium sodium niobate (KNN) single crystals and polycrystals: a comparison study. *Cryst Growth Des* 15:1289–94
9. Lin C-C, Su C-W, Weng C-M, Chien Y-C, Chu S-Y, Huang C-Y et al. (2018) Effects of two-stage post-annealing process on microstructure and electrical properties of sol-gel derived non-stoichiometric NKN thin films. *Appl Surf Sci* 428:199–206
10. Ullah A, Alam M, Ullah A, Ahn CW, Lee J-S, Cho S et al. (2016) High strain response in ternary  $\text{Bi}_{0.5}\text{Na}_{0.5}\text{TiO}_3$ ,  $\text{BaTiO}_3$ ,  $\text{Bi}(\text{Mn}_{0.5}\text{Ti}_{0.5})\text{O}_3$  solid solutions. *RSC Adv* 6:63915–21
11. Choudhary R, Perez K, Bhattacharya P, Katiyar R (2007) Structural and dielectric properties of mechanochemically synthesized  $\text{BiFeO}_3$ ,  $\text{Ba}(\text{Zr}_{0.6}\text{Ti}_{0.4})\text{O}_3$  solid solutions. *Mater Chem Phys* 105:286–92
12. Maniammal K, Madhu G, Biju V (2017) X-ray diffraction line profile analysis of nanostructured nickel oxide: shape factor and convolution of crystallite size and microstrain contributions. *Phys E Low-Dimens Syst Nanostruct* 85:214–22
13. Zak AK, Majid WA, Abrishami ME, Yousefi R (2011) X-ray analysis of ZnO nanoparticles by Williamson, Hall and size, strain plot methods. *Solid State Sci* 13:251–6
14. Mote V, Purushotham Y, Dole B (2012) Williamson–Hall analysis in estimation of lattice strain in nanometer-sized ZnO particles. *J Theor Appl Phys* 6:6
15. Lal M, Shandilya M, Kumar AS, Rai R, Nair SS, Palai R (2018) Study of structural and magnetoelectric properties of  $(1-x)(\text{Ba}_{0.96}\text{Ca}_{0.04}\text{TiO}_3)_x(\text{ZnFe}_2\text{O}_4)$  ceramic composites. *J Mater Sci Mater Electron* 29:80–5
16. Dai Y, Zhang X, Zhou G (2007) Phase transitional behavior in  $\text{K}_{0.5}\text{Na}_{0.5}\text{NbO}_3$ ,  $\text{LiTaO}_3$  ceramics. *Appl Phys Lett* 90:262903
17. Aydin C, Al-Hartomy OA, Al-Ghamdi A, Al-Hazmi F, Yahia I, El-Tantawy F et al. (2012) Controlling of crystal size and optical band gap of CdO nanopowder semiconductors by low and high Fe contents. *J Electroceram* 29:155–62
18. Vineeshkumar T, Raj DR, Prasanth S, Unnikrishnan N, Pillai VM, Sudarasanakumar C (2018) Fe induced optical limiting properties of  $\text{Zn}_{1-x}\text{Fe}_x\text{S}$  nanospheres. *Opt Laser Technol* 99:220–9
19. Yao T, An X, Han H, Chen JQ, Li C (2018) Photoelectrocatalytic materials for solar water splitting *Adv Energy Mater* 8(21):1800210
20. Wang L, Zuo R, Liu L, Su H, Shi M, Chu X et al. (2011) Preparation and characterization of sol-gel derived (Li, Ta, Sb) modified (K, Na)  $\text{NbO}_3$  lead-free ferroelectric thin films. *Mater Chem Phys* 130:165–9
21. Ahn C, Lee S, Lee H, Ullah A, Bae J, Jeong E et al. (2009) The effect of K and Na excess on the ferroelectric and piezoelectric properties of  $\text{K}_{0.5}\text{Na}_{0.5}\text{NbO}_3$  thin films. *J Phys D Appl Phys* 42:215304